Continuous-wave and Q-switched microchip laser performance of Yb:$Y_3Sc_2Al_3O_{12}$ crystals

Jun Dong[1,*], Ken-ichi Ueda[1], and Alexander A. Kaminskii[2]

[1]*Institute for Laser Science, University of Electro-Communications, 1-5-1 Chofugaoka, Chofu, Tokyo 182-8585, Japan*
[2]*Institute of Crystallography, Russian Academy of Sciences, Leninskii Prospekt 59, Moscow 119333, Russia*
**Corresponding author: j.dong@hw.ac.uk or jundong_99@yahoo.com*

Abstract: Optical properties of Yb:$Y_3Sc_2Al_3O_{12}$ crystal were investigated and compared with those from Yb:YAG crystals. The broad absorption and emission spectra of Yb:$Y_3Sc_2Al_3O_{12}$ show that this crystal is very suitable for laser-diode pumping and ultrafast laser pulse generation. Laser-diode pumped continuous-wave and passively Q-switched Yb:$Y_3Sc_2Al_3O_{12}$ lasers with Cr^{4+}:YAG crystals as saturable absorber have been demonstrated for the first time. Continuous-wave output power of 1.12 W around 1032 nm (multi-longitudinal modes) was measured with an optical-to-optical efficiency of 30%. Laser pulses with pulse energy of over 31 μJ and pulse width of 2.5 ns were measured at repetition rate of over 12.7 kHz; a corresponding peak power of over 12 kW was obtained. The longitudinal mode selection by a thin plate of Cr^{4+}:YAG as an intracavity etalon was also observed in passively Q-switched Yb:$Y_3Sc_2Al_2O_{12}$ microchip lasers.

OCIS codes: (140.3380) Laser materials; (140.3480) Lasers, diode-pumped; (140.3540) Lasers, Q-switched; (140.5680) Rare earth and transition metal solid-state lasers.

References and links

1. W. F. Krupke, "Ytterbium solid-state lasers - The first decade," IEEE J. Sel. Top. Quantum Electron. **6**, 1287 - 1296 (2000).
2. J. Dong, A. Shirakawa, K. Ueda, H. Yagi, T. Yanagitani, and A. A. Kaminskii, "Efficient Yb^{3+}:$Y_3Al_5O_{12}$ ceramic microchip lasers," Appl. Phys. Lett. **89**, 091114 (2006).
3. C. Honninger, R. Paschotta, M. Graf, F. Morier-Genoud, G. Zhang, M. Moser, S. Biswal, J. Nees, A. Braun, G. A. Mourou, I. Johannsen, A. Giesen, W. Seeber, and U. Keller, "Ultrafast ytterbium-doped bulk lasers and laser amplifiers," Appl. Phys. B **69**, 3 - 17 (1999).
4. P. Lacovara, H. K. Choi, C. A. Wang, R. L. Aggarwal, and T. Y. Fan, "Room-temperature diode-pumped Yb:YAG laser," Opt. Lett. **16**, 1089 - 1091 (1991).
5. U. Brauch, A. Giesen, M. Karszewski, C. Stewen, and A. Voss, "Multiwatt diode-pumped Yb:YAG thin disk laser continuously tunable between 1018 and 1053 nm," Opt. Lett. **20**, 713 - 715 (1995).
6. T. Taira, J. Saikawa, T. Kobayashi, and R. L. Byer, "Diode-pumped tunable Yb:YAG miniature lasers at room temperature: modeling and experiment," IEEE J. Sel. Top. Quantum Electron. **3**, 100 - 104 (1997).
7. H. W. Bruesselbach, D. S. Sumida, R. A. Reeder, and R. W. Byren, "Low-heat high-power scaling using InGaAs-diode-pumped Yb:YAG lasers " IEEE J. Sel. Top. Quantum Electron. **3**, 105 - 116 (1997).
8. G. A. Bogomolova, D. N. Vylegzhanin, and A. A. Kaminskii, "Spectral and lasing investigations of garnets with Yb^{3+} ions," Sov. Phys. JETP **42**, 440 - 446 (1976).
9. T. H. Allik, C. A. Morrison, J. B. Gruber, and M. R. Kokta, "Crystallography, spectroscopic analysis, and lasing properties of Nd^{3+}:$Y_3Sc_2Al_3O_{12}$," Phys. Rev. B **41**, 21 - 30 (1990).
10. Y. Sato, T. Taira, and A. Ikesue, "Spectral parameters of Nd^{3+}-ion in the polycrystalline solid-solution composed of $Y_3Al_5O_{12}$ and $Y_3Sc_2Al_3O_{12}$," Jpn. J. Appl. Phys. **42** (2003).
11. M. Kokta, "Solubility enhancement of Nd^{3+} in scandium-substituted rare earth-aluminum garnets," J. Solid State Chem. **8**, 39 -42 (1973).
12. A. A. Kaminskii, *Laser Crystals* (Springer-Verlag, Berlin Heidelberg New York, 1981).
13. A. A. Kaminskii, and L. Li, "Analysis of spectral line intensities of TR^{3+} ions in disordered crystal systems," Phys. Status Solidi (a) **26**, K21 - K26 (1974).
14. J. Dong, A. Rapaport, M. Bass, F. Szipocs, and K. Ueda, "Temperature-dependent stimulated emission cross section and concentration quenching in highly doped Nd^{3+}:YAG crystals," Phys. Status Solidi (a) **202**, 2565 - 2573 (2005).

#92201 - $15.00 USD Received 28 Jan 2008; revised 18 Mar 2008; accepted 24 Mar 2008; published 1 Apr 2008

15. J. Saikawa, Y. Sato, T. Taira, and A. Ikesue, "Absorption, emission spectrum properties, and efficient laser performances of Yb:$Y_3ScAl_4O_{12}$ ceramics," Appl. Phys. Lett. **85**, 1898 -1900 (2004).
16. J. Saikawa, Y. Sato, and T. Taira, "Passively mode locking of a mixed garnet Yb:$Y_3ScAl_4O_{12}$ ceramic laser," Appl. Phys. Lett. **85**, 5845 - 5847 (2004).
17. J. Dong, M. Bass, Y. Mao, P. Deng, and F. Gan, "Dependence of the Yb^{3+} emission cross section and lifetime on the temperature and concentration in ytterbium aluminum garnet," J. Opt. Soc. Am. B **20**, 1975 - 1979 (2003).
18. S. Kuck, K. Petermann, U. Pohlmann, U. Schonhoff, and G. Huber, "Tunable room-temperature laser action of Cr^{4+}-doped $Y_3Sc_xAl_{5-x}O_{12}$," Appl. phys. B **58**, 153 - 156 (1994).
19. D. S. Sumida, and T. Y. Fan, "Effect of radiation trapping on fluorescence lifetime and emission cross section measurements in solid-state laser media " Opt. Lett. **19**, 1343 - 1345 (1994).
20. F. Salin, and J. Squier, "Gain guiding in solid-state lasers," Opt. Lett. **17**, 1352 - 1354 (1992).
21. E. J. Grace, G. H. C. New, and P. M. W. French, "Simple *ABCD* matrix treatment for transversely varying saturable gain," Opt. Lett. **26**, 1776 - 1778 (2001).
22. J. K. Jabczynski, J. Kwiatkowski, and W. Zendzian, "Modeling of beam width in passively *Q*-switched end-pumped lasers," Opt. Express **11**, 552 - 559 (2003).
23. J. Dong, and K. Ueda, "Observation of repetitively nanosecond pulse-width transverse patterns in microchip self-Q-switched laser," Phys. Rev. A **73**, 053824 (2006).
24. J. J. Degnan, "Optimization of passively Q-switched lasers," IEEE J. Quantum Electron. **31**, 1890 - 1901 (1995).
25. J. Dong, A. Shirakawa, and K. Ueda, "Sub-nanosecond passively Q-switched Yb:YAG/Cr^{4+}:YAG sandwiched microchip laser," Appl. Phys. B: Lasers Opt. **85**, 513 - 518 (2006).
26. W. Koechner, *Solid State Laser Engineering* (Springer-Verlag, Berlin, 1999).
27. W. P. Risk, "Modeling of longitudinally pumped solid-state lasers exhibiting reabsorption losses," J. Opt. Soc. Am. B **5**, 1412 -1423 (1988).
28. J. Dong, A. Shirakawa, and K. Ueda, "Switchable pulses generation in passively Q-switched multilongitudinal-mode microchip laser," Laser Phys. Lett. **4**, 109 - 116 (2007).

1. Introduction

Ytterbium doped laser materials have been intensely investigated for developing high power laser-diode pump solid-state lasers, tunable lasers and femtosecond lasers around 1 μm [1-3]. Yb:YAG as crystals and polycrystalline ceramics are one of the dominant laser gain media used for solid-state lasers [4-7] owing to the excellent optical, thermal, chemical and mechanical properties [8]. In particular, partial-substitution of Sc^{3+} for Al^{3+} in $Y_3Al_5O_{12}$ crystal or ceramics to form distorted $Y_3Sc_xAl_{5-x}O_{12}$ structure provides $Y_3Sc_xAl_{5-x}O_{12}$ compounds with preferable conditions for trivalent lanthanide (Ln^{3+}) lasant doping. There are several reports of the optical properties and laser performance of Nd:$Y_3Sc_2Al_3O_{12}$ (YSAG) crystals and ceramics [9, 10]. The distribution coefficient for Nd^{3+} in YSAG is roughly twice that in YAG [11], making it possible to increase the Nd^{3+} concentration in YSAG over that in YAG. Replacing Al^{3+} ions with larger Sc^{3+} ions in a YAG host increases the distance between dodecahedral lattice sites (substitutional sites for Nd^{3+} ions in the garnet structure). Any increase in separation between neighboring Nd^{3+} ions, especially with increasing Nd^{3+} concentration in YAG, tends to reduce the relatively strong ion-ion interaction in YAG, which leads to concentration quenching of the Nd^{3+} fluorescence [12-14]. In addition, the aluminum-based systems, such as YAG, YSAG, or gadolinium scandium aluminum garnet (GSAG), are formed from more stable constituent oxides than gallium-containing materials, such as GGG. The tendency for color center formation in gallium-containing garnets is due to oxidation state variation or oxygen vacancies, and this problem is greatly reduced in aluminate systems. With substituting of Al^{3+} ions with Sc^{3+} ions in YSAG crystal, the refractive index of YSAG crystal was measured to be 1.873 at 632.8 nm, which is higher than that for YAG crystal [9]. The thermal and mechanical properties of YSAG crystals or ceramics by partially replacing Al^{3+} ions with Sc^{3+} ions are still comparable to that of YAG crystal or ceramics. And the optical spectra of Nd:YSAG crystal become relative broader compared to those from Nd:YAG crystal. There are also some reports on the optical properties and laser performance of $Y_3ScAl_4O_{12}$ ceramics doped with Nd^{3+} or Yb^{3+} ions [10, 15, 16]. The broad absorption and emission spectra were obtained by enlarging the distance between dodecahedral lattice sites by introducing large Sc^{3+} ions in $Y_3ScAl_4O_{12}$ ceramics doped with Nd^{3+} or Yb^{3+} ions. However, for Yb:$Y_3ScAl_4O_{12}$ ceramic, the emission cross-section is only 1.4×10^{-20} cm^2 [15],

#92201 - $15.00 USD Received 28 Jan 2008; revised 18 Mar 2008; accepted 24 Mar 2008; published 1 Apr 2008

which is lower than that for Yb:YAG crystal (about 2.3×10^{-20} cm^2 [17]). Up to now, there has been no report on the optical properties of Yb:YSAG crystal or ceramics although the optical properties and thermal properties are assumed to be better or comparable to those of Yb:YAG crystals or ceramics. By the introduction of more Sc ions in Yb:YSAG crystals, more broader absorption and emission spectra were expected and are more suitable for laser-diode pumping and ultrashort pulse generation. Therefore, it is worth examining the optical properties and laser properties of Yb:YSAG crystals from the point of view of both scientific research and laser-diode pumped solid-state laser applications.

Here, we report, for the first time to our knowledge, the optical properties of Yb:YSAG crystals and continuous-wave and passively Q-switched Yb:YSAG microchip laser operation with Cr^{4+}:YAG as a saturable absorber. The broad absorption and emission spectra of Yb:YSAG crystals were measured and compared to those of Yb:YAG crystals and Yb:$Y_3ScAl_4O_{12}$ ceramics. Continuous-wave and passively Q-switched laser operation also show that Yb:YSAG crystals can generate laser emission with wide bandwidth (2 nm wide with multi-longitudinal-mode oscillation), providing evidence of suitability for generating ultrashort pulse with YbYSAG crystal as gain medium.

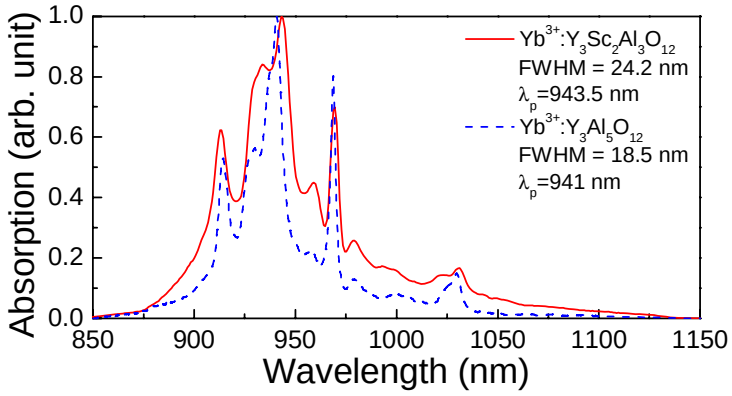

Fig. 1. Absorption spectrum of Yb:YSAG crystals doped with 5 at.% Yb^{3+}-ions at room temperature, the absorption spectrum of Yb:YAG doped with 5 at.% Yb^{3+}-ions is also plotted for comparison.

2. Optical properties of Yb:YSAG crystal

The Yb:YSAG crystal used in the experiments was grown by traditional Czochralski (CZ) method, with a Yb^{3+}-ion doping concentration of 5 at.%. The crystal was grown along the <111> axis direction. The absorption and emission spectra of Yb:YSAG crystal were measured at room temperature. A Yb:YAG crystal doped with 5 at.% Yb was also used to compare the optical properties with those of Yb:YSAG crystals. The absorption spectra of Yb:YSAG and Yb:YAG crystals are shown in Fig. 1. The absorption characteristics of Yb:YSAG crystal are similar to those of Yb:YAG crystals. There are four absorption peaks centered at 914, 943.5, 969 and 1031 nm, respectively. 914, 943.5 and 969 nm are suitable for laser-diode pumping. The absorption coefficient at 943.5 nm is 4 cm^{-1}. However, the peak absorption wavelength centered at 943.5 nm is about 2.5 nm red-shift comparing to that for Yb:YAG crystal. The emission shift to longer wavelength of Yb:YSAG crystal is caused by the weakening of crystal field by the substitution of the Al^{3+} ion by larger Sc^{3+} ions [18]. The absorption bandwidth (FWHM) of Yb:YSAG crystals centered at 943.5 nm was measured to be 24.2 nm, which is about 1.3 times wider than that for Yb:YAG crystals and 2.2 nm wider than that of Yb:$Y_3ScAl_4O_{12}$ ceramics [15]. Therefore, the Yb:YSAG crystal is more suitable for 940-nm laser-diode pumping owing to the broader band absorption features. Figure 2

#92201 - $15.00 USD Received 28 Jan 2008; revised 18 Mar 2008; accepted 24 Mar 2008; published 1 Apr 2008

shows the room temperature emission spectra of Yb:YSAG crystals containing 5 at.% of ytterbium activators. The emission spectra of Yb:YSAG crystal is similar to that of Yb:YAG single crystals. Two main emission peaks are centered at 1031.4 nm and 1050 nm, the effective emission intensity at 1031.4 nm is about 6 times of that at 1050 nm. The emission bandwidth centered at 1031.4 nm (~ 14 nm) was about 1.6 times wider than that of Yb:YAG crystal and also 1.5 nm wider than that of Yb:$Y_3ScAl_4O_{12}$ ceramics (~ 12 nm [15]). The fluorescence lifetime was measured to be 1.1 ms owing to the radiative trapping effect in the lifetime measurement for ytterbium doped materials, which is similar to that of Yb:$Y_3ScAl_4O_{12}$ ceramics [15] and longer than that of Yb:YAG crystals (~ 0.951 ms [17, 19]).

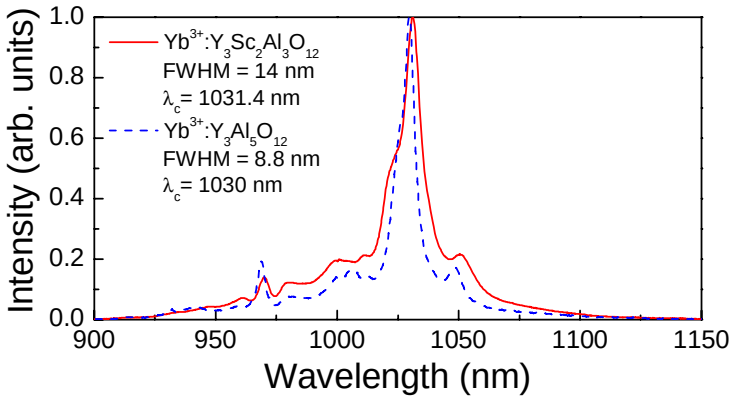

Fig. 2. Emission spectrum of Yb:YSAG crystals doped with 5 at.% Yb^{3+}-ions at room temperature. The emission spectrum of Yb:YAG crystal is shown for comparison.

The absorption cross-section spectrum of Yb:YSAG crystals was calculated by using the absorption spectrum of Yb:YSAG and the concentration of Yb^{3+}-ion in the Yb:YSAG crystal. The effective emission cross-section spectrum was estimated by using the Fuchtbauer-Ladenburg (F-L) formula and measured fluorescence lifetime of the Yb:YSAG crystal. Therefore, the gain cross-section of the Yb:YSAG crystal was determined from the absorption and emission cross-section spectra of Yb:YSAG crystal under different population inversion rate, $\beta = N_2/N_0$, N_2 is the inversion population and N_0 is the total population of Yb^{3+}-ions in Yb:YSAG crystal. The gain cross-section spectra of Yb:YSAG can be expressed as $\sigma_g(\lambda) = \beta\sigma_e(\lambda) - (1 - \beta)\sigma_a(\lambda)$. $\sigma_e(\lambda)$ and $\sigma_a(\lambda)$ are the emission and absorption cross-section of the Yb:YSAG crystal, respectively. Figure 3 shows the gain cross-section, $\sigma_g(\lambda)$, of Yb:YSAG crystal for different values of population inversion rate, β. The absorption cross-section spectrum was obtained when β was set to 0; and the emission cross-section spectrum was obtained when β was set to 1. Absorption cross-section peak is located near 943.5 nm, with a value of 0.73×10^{-20} cm^2, and emission cross-section peak is located near 1031.4 nm, with a value of ~ 1.8×10^{-20} cm^2, which is lower than that of Yb:YAG crystal (about 2.3×10^{-20} cm^2) [17] and higher than that of Yb:$Y_3ScAl_4O_{12}$ ceramics (~ 1.4×10^{-20} cm^2) [15]. It is worth noting that there is another absorption peak near 969 nm, which is also useful for optical pumping for realizing high quantum efficiency laser operation. We also note that the emission spectrum extends up to nearly 1100 nm, which is promising for the development of new broadly tunable laser sources, as well as for the design of femtosecond oscillators or amplifiers.

#92201 - $15.00 USD Received 28 Jan 2008; revised 18 Mar 2008; accepted 24 Mar 2008; published 1 Apr 2008

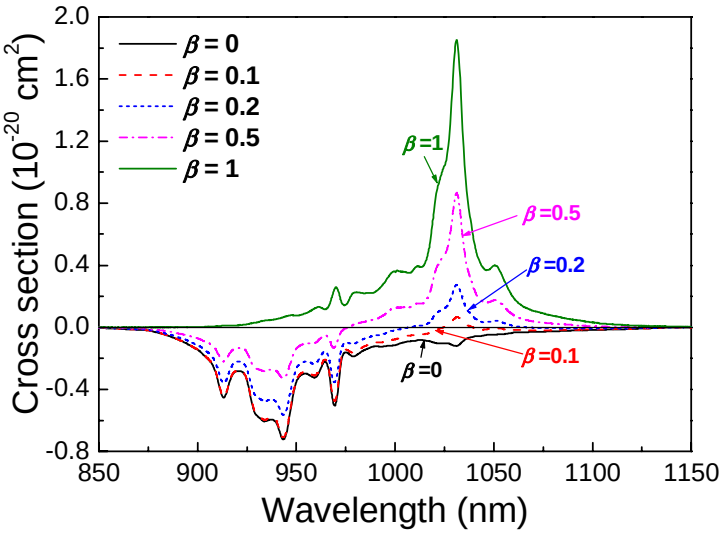

Fig. 3. Gain cross-section, $\sigma_g(\lambda)$ of Yb:YSAG crystals for different values of population inversion rate, $\beta = N_2/N_0$. $\sigma_g(\lambda) = \beta\sigma_e(\lambda) - (1 - \beta)\sigma_a(\lambda)$. $\sigma_e(\lambda)$ and $\sigma_a(\lambda)$ are the emission and absorption cross-section of Yb:YSAG crystals, respectively. Absorption cross-section spectrum was obtained when β was set to 0; emission cross-section spectrum was obtained when β was set to 1.

3. Laser experiments

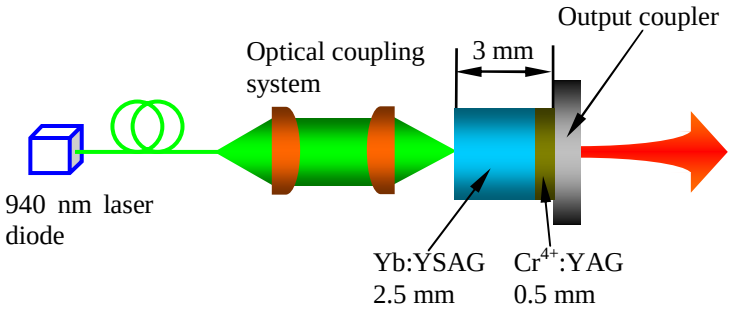

Fig. 4. Schematic diagram for laser-diode end-pumped continuous-wave and passively Q-switched Yb:YSAG microchip lasers with Cr^{4+}:YAG as saturable absorber.

Figure 4 shows a schematic diagram of room temperature continuous-wave and passively Q-switched Yb:YSAG microchip lasers with a Cr^{4+}:YAG crystal as saturable absorber. The gain medium is a plane-parallel coated Yb:YSAG crystal, and the thickness of the crystal is 2.5 mm. The concentration of Yb^{3+}-dopants in the Yb:YSAG crystal is 5 at.%. One surface of the Yb:YSAG crystal is coated for high transmission at 940 nm and total reflection at 1030 nm lasing wavelength, acting as one mirror of the resonator. The other surface of the Yb:YSAG crystal is antireflection coated for 1030 nm lasing wavelength to reduce the intracavity loss. Two plane-parallel output coupling mirrors with 5 and 10% transmission (T_{oc}) at 1030 nm were used as output couplers. The cavity length is the thickness of the Yb:YSAG crystal, e.g. about 2.5 mm. For passively Q-switched operation, one 0.5-mm-thick Cr^{4+}:YAG crystal with

#92201 - $15.00 USD Received 28 Jan 2008; revised 18 Mar 2008; accepted 24 Mar 2008; published 1 Apr 2008

initial transmission of 95% was sandwiched between Yb:YSAG crystal and output coupler with 10% transmission to avoid coating damage. A high-power fiber-coupled 940 nm laser-diode with a core diameter of 100 μm and numerical aperture of 0.22 was used as the pump source. Two lenses of 8 mm focal length were used to focus the pump beam on the crystal rear surface and to produce a pump light spot on the crystal of about 100 μm in diameter. The laser was operated at room temperature without active cooling of the working parts. The Q-switched pulse shapes were recorded by using a fiber-coupled InGaAs photodiode with a bandwidth of 16 GHz and a 7 GHz Tektronix TDS7704B digital phosphor oscilloscope. The stimulated emission ($^2F_{5/2}\rightarrow{}^2F_{7/2}$ channel) spectrum was analyzed by using an optical spectrum analyzer. The laser output beam profile was monitored using a CCD camera both in the near field and the far field of the output coupler.

4. Results and discussion

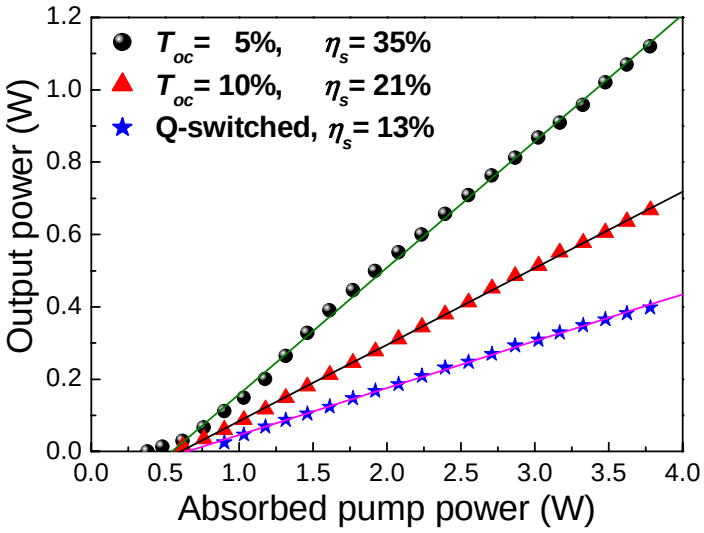

Fig. 5. Continuous-wave output power of Yb:YSAG microchip lasers as a function of absorbed pump power under different output couplings (T_{oc} = 5 and 10%) and average output power as a function of the absorbed pump power for passively Q-switched Yb:YSAG microchip lasers with Cr^{4+}:YAG as saturable absorber.

Absorbed pump power of the Yb:YSAG crystal was obtained by measuring the incident pump power after the coupling optics and the residual power after the Yb:YSAG crystal and the output coupler under lasing condition. The absorption efficiency of Yb:YSAG crystal under no-lasing condition without output coupler was measured to be 62% for available maximum incident pump power of 6.3 W, which is very close to the absorption efficiency calculated by adopting Beer's law. The absorption efficiency of Yb:YSAG crystal nearly keeps constant under lasing condition. However, the absorption efficiency will decrease when the pump power is much higher than the present pump power level, because the thermal effect will be the main factor in changing the absorption coefficient of Yb:YSAG crystal. The absorption efficiency in passively Q-switching operation of Yb:YSAG/Cr^{4+}:YAG microchip laser was higher than that in free-running operation because there is absorption from the Cr^{4+}:YAG crystal part of the Yb:YSAG/Cr^{4+}:YAG microchip laser. The pump power absorbed by the Cr^{4+}:YAG crystal is less than 1.3%, estimated from the thickness and absorption coefficient at 940 nm of Cr^{4+}:YAG crystal. The pump power intensity (estimated to be less than 1 kW/cm^2) in Cr^{4+}:YAG crystal is too low to modulate the absorption of Cr^{4+}:YAG crystal, so, the effect

#92201 - $15.00 USD Received 28 Jan 2008; revised 18 Mar 2008; accepted 24 Mar 2008; published 1 Apr 2008

of the absorption of pump power in the Cr^{4+}:YAG crystal on passively Q-switched laser performance can be neglected. The output power of continuous-wave operation for different output couplings and the average output power of passively Q-switched Yb:YSAG microchip lasers as a function of the absorbed pump power are shown in Fig. 5. For continuous-wave laser operation, the absorbed pump power thresholds are 0.38, 0.56 W for T_{oc} = 5, and 10%. The output power is observed to increase linearly with the absorbed pump power, and to decrease with an increase of the transmission of output couplers. The slope efficiencies were measured to be 35, and 21 % for T_{oc} = 5, and 10 %. Maximum output power of 1.12 W was measured with T_{oc} = 5% at absorbed pump power of 3.78 W, corresponding to optical-to-optical efficiency of 30%. The low optical-to-optical efficiencies in free running Yb:YSAG microchip lasers with different output coupling may be caused by the low doping concentration of Yb^{3+}-ion in the YSAG crystal. Although a thick crystal (2.5 mm) was used in the laser experiments, and over 60% of the pump power was absorbed by the crystal, the bad beam quality from laser-diode cause insufficient usage of the incident pump power on the crystal; and some of the pump power absorbed at the exit side of the Yb:YSAG crystal can not excite enough population inversion inside the gain medium, therefore, the laser optical-to-optical efficiency is low. The laser performance of the Yb:YSAG crystal can be further improved by using a thin crystal with high doping concentration, which will provide good overlap between the pump beam and the laser beam in laser-diode end-pumped microchip lasers. Increase pump beam diameter incident on Yb:YSAG crystal will be another way to improve the laser performance. The pump power intensity at maximum available pump power of 6.3 W was calculated to be 80 kW/cm^2 in our present experiments, which was about 3 times higher than the saturation intensity (about 26.2 kW/cm^2) of absorption centered at 943.5 nm for Yb:YSAG crystal. Therefore, the lasers operated in the regime of strongly saturated absorption and saturated gain, the transverse modes formation is governed by the saturated gain-guided process both for free-running and Q-switched operations [20-23]. However, we did not observed multi-transverse modes oscillation in our lasers even in available highest pump power intensity, the lasers oscillated in fundamental TEM_{00} mode. The fundamental mode radius close to the output coupler for these lasers was measured to be 50 μm, and near-diffraction-limited beam quality with M^2 less than 1.2 was achieved in continuous-wave and passively Q-switched Yb:YSAG/Cr^{4+}:YAG microchip lasers. The causes of fundamental mode oscillation in these lasers under saturated absorption were owing to the nature of Yb^{3+} ions in YSAG crystal, the Yb^{3+}-ions have strong reabsorption at lasing wavelength around 1030 nm as shown in Fig. 1. Because the pump beam profile from fiber-coupled laser-diode in our experiments is close to Gaussian distribution, the pump power intensity distribution along the radius decreases from the center to the edge of the pump beam spot in the crystal, therefore, the inversion population at the edge of the pump spot in the gain medium is small, which is not high enough to overcome the threshold for multimode oscillation even with saturated gain-guiding effect. Thus, we did not observe multi-transverse modes oscillation in our Yb:YSAG lasers at highest pump power intensity. Increase pump beam diameter with top-hat beam profile makes the pump power distribution inside the gain medium more uniform and multimode oscillation. The efficiency of lasers could be increased with large pump beam diameter under certain pump power levels compared to that with tightly focus beam.

The pump power thresholds were about 0.76 W for passively Q-switched laser operation with T_0 = 95 %. The average output power increases linearly with absorbed pump power. There was no pump saturation; the output power can be further scaled with high pump power. The slope efficiencies (η_s) were measured to be about 13% for T_0 = 95 %. A maximum average output power of 400 mW was measured when the absorbed pump power was 3.78 W for T_0 = 95 %. The corresponding optical-to-optical efficiency of 11% was achieved for T_0 = 95 %. The optical-to-optical efficiency can be further increased by using a Cr^{4+}:YAG crystal with high initial transmission. However, the pulse energy will be decreased and pulse width will be increased with high initial transmission of Cr^{4+}:YAG crystals [24]. In practice, the initial transmission of Cr^{4+}:YAG can be chosen to realize different pulse energy values and repetition rates depending on the required applications of such lasers.

#92201 - $15.00 USD Received 28 Jan 2008; revised 18 Mar 2008; accepted 24 Mar 2008; published 1 Apr 2008

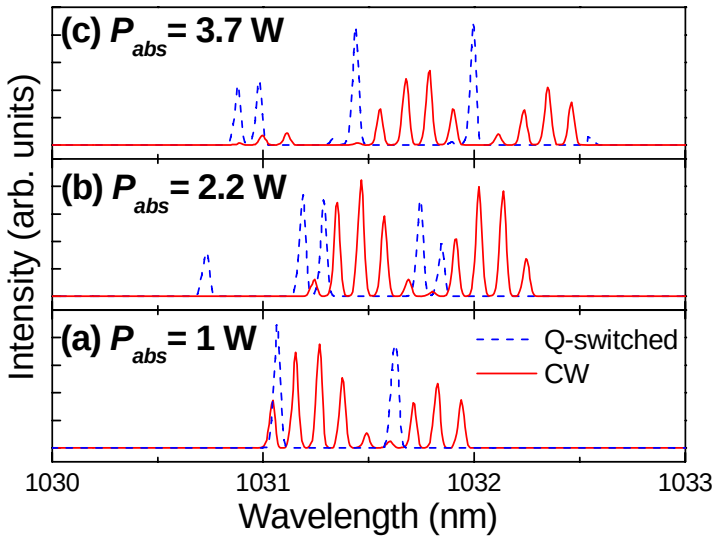

Fig. 6. Stimulated emission spectra for different pump powers in continuous-wave and passively Q-switched Yb:YSAG microchip lasers with Cr^{4+}:YAG as the saturable absorber.

Continuous-wave and passively Q-switched Yb:YSAG microchip lasers operate in a TEM_{00} mode with multi-longitudinal modes owing to the broad emission spectrum of the Yb:YSAG crystal. Stimulated emission (SE) indicated that the continuous-wave laser operates in three to twelve longitudinal-modes and the passively Q-switched Yb:YSAG/Cr^{4+}:YAG microchip laser oscillates in two- to six- longitudinal-modes depending on the pump power levels. Figure 6 shows the SE spectra of continuous-wave and Q-switched Yb:YSAG microchip lasers with T_0 = 95% Cr^{4+}:YAG as saturable absorber for T_{oc} = 10% under different pump power levels. For continuous-wave operation, the axial laser modes increase with the absorbed pump power, and there is mode competition and mode hopping owing to the strong competition for the inversion population at different resonant frequencies. The central wavelength around 1031.4 nm shifts with pump power to longer wavelengths. This is caused by the temperature dependent emission spectrum of Yb:YSAG crystal, exhibiting the same properties as those of Yb:YAG crystals [17]. However, at high pump power levels (e.g. over 2.5 W), some longitudinal modes appear at short wavelength [as shown in Fig. 6(c)] owing to the asymmetric broad emission spectra of Yb:YSAG crystal and due to the high population inversion, so that several possible resonant frequencies compete each other, leading to the observation of broad emission spectra of the laser.

For passively Q-switched laser operation, single longitudinal mode oscillation was not observed even when the laser was oscillating just above the lasing threshold. However, the single-longitudinal-mode oscillation in passively Q-switched Yb:YAG/Cr^{4+}:YAG microchip lasers was observed [25]. From these results of laser emission spectra for passively Q-switched Yb:YAG and Yb:YSAG microchip lasers, we can see that broad emission spectra of Yb:YSAG crystal is more suitable for broad tunable laser operations. Two longitudinal-modes were obtained when the absorbed pump power was above the threshold and set below 1.5 W. The resonant modes oscillate at 1031.06 and 1031.622 nm due to the asymmetric gain profile centered at 1031.4 nm and mode-selection effect of the Cr^{4+}:YAG etalon. The separation between longitudinal modes was measured to be 0.568 nm, which is five times wider than those of continuous-wave oscillation and six times wider than the free spectral range between the resonant modes (0.094 nm) in the laser cavity filled with gain medium predicted by [26] $\Delta\lambda_c = \lambda^2/2L_c$, where L_c is the optical length of the resonator and λ is the laser wavelength. The

#92201 - $15.00 USD Received 28 Jan 2008; revised 18 Mar 2008; accepted 24 Mar 2008; published 1 Apr 2008

potential output longitudinal modes were selected by the combined etalon effect of the 0.5-mm-thick Cr:YAG crystal as an intracavity etalon and 2.5-mm-thick Yb:YSAG lasing section as a resonant reflector. Five longitudinal-modes dominated in the high pump power regime [e.g. P_{abs} > 2 W, as shown in Fig. 6(b)]. The interesting phenomenon is that the third- and fourth- modes appear at 1031.286 and 1031.844 nm and fifth-mode appears at 1030.734 nm when the pump power is 2.2 W. This may be caused by the asymmetric gain distribution of Yb:YSAG crystal and the resonant mode competition for the saturated inversion population which is strongly dependent on the intracavity laser intensity [27]. Therefore, competition between the gain provided by the saturated inversion population and losses from the gain profile under high temperature due to the absorbed pump power [8] will dominate the stimulated emission spectra. For further increase of the pump power, there is strong mode competition and mode hopping as shown in Fig. 6(c). The linewidth of each mode was less than 5.7 GHz, limited by the resolution of the available optical spectra analyzer. The central wavelength of 1031.4 nm shifts to longer wavelength with pump power, which is caused by the temperature dependent emission spectrum of Yb:YSAG crystal, the same properties as that of Yb:YAG crystals [17].

For multi-longitudinal-mode oscillation of passively Q-switched Yb:YSAG/Cr^{4+}:YAG microchip lasers, the output pulses from different longitudinal modes are governed by the gain coefficient distribution for each mode, intracavity loss, and gain competition inside the laser Fabry-Perot cavity among different modes. The time interval of the total output pulse trains is determined by the bleaching and recovery of the saturable absorber, which is strongly dependent on the pump power level.

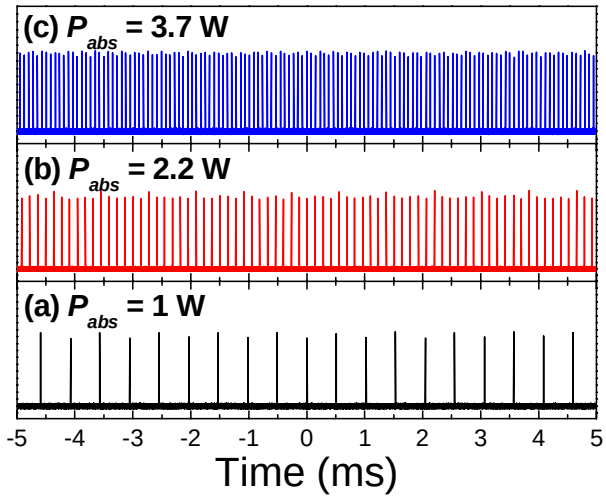

Fig. 7. Some typical output pulse trains of the passively Q-switched Yb:YSAG microchip lasers with Cr^{4+}:YAG as saturable absorber under the different pump power levels, which correspond to the stimulated emission spectra in Fig. 6.

Figure 7 shows oscilloscope traces of the pulse trains under different absorbed pump power levels, indicating that the pulse train characteristics. The output pulse trains vary with the pump power. At low pump power levels, there are two pulses oscillating alternatively with different pulse amplitudes [as shown in Fig. 7(a)], and exhibiting antiphase dynamics, which is also observed in passively Q-switched Yb:YAG/Cr^{4+}:YAG microchip lasers [28]. For further increases of the pump power, additional longitudinal modes oscillate and the pulse trains become more complex. When the laser oscillates on five longitudinal modes at absorbed pump power of 2.2 W, the output laser pulse train exhibits period-6 modulated oscillation as shown in Fig. 7(b). Owing to the strong mode competition and mode hopping in

#92201 - $15.00 USD Received 28 Jan 2008; revised 18 Mar 2008; accepted 24 Mar 2008; published 1 Apr 2008

the output laser spectra [as shown in Fig. 6(c)], the corresponding output pulse trains tends to become more stable comparing those obtained at low pump power levels. The output pulse amplitudes and repetition rate fluctuations are less than 10% [as shown in Fig. 7(c)], evidencing relatively stable passively Q-switching laser operation.

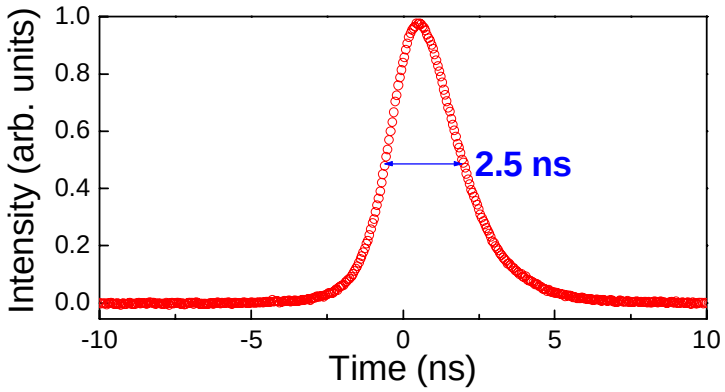

Fig. 8. Passively Q-switched Yb:YSAG microchip laser pulse with 2.5 ns pulse width (FWHM) and 30 μJ pulse energy, corresponding to peak power of over 12 kW.

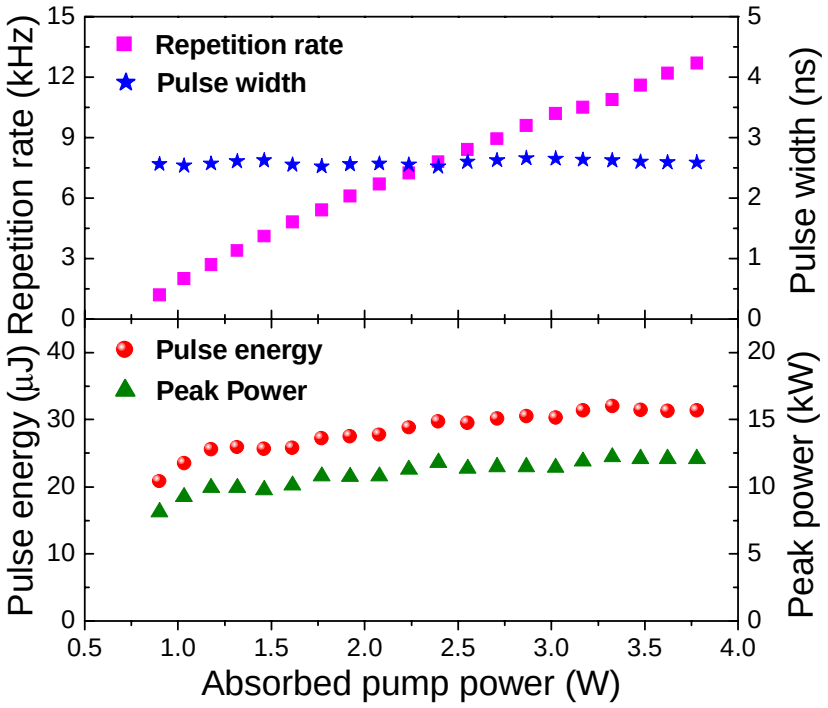

Fig. 9. The pulse characteristics (pulse energy, pulse width, repetition rate and peak power) of laser-diode pumped passively Q-switched Yb:YSAG microchip lasers with Cr^{4+}:YAG as saturable absorber as a function of absorbed pump power.

#92201 - $15.00 USD Received 28 Jan 2008; revised 18 Mar 2008; accepted 24 Mar 2008; published 1 Apr 2008

Although there is some fluctuations (including repetition timing jitter and pulse amplitude fluctuation) in the output pulse trains, the output pulse profile remains nearly the same, Figure 8 shows a typical pulse profile obtained at an absorbed pump power of 3.78 W. Over 12 kW peak power laser pulses with a pulse width of 2.5 ns and pulse energy of 31 μJ were obtained at a repetition rate of 12.7 kHz when the absorbed pump power is 3.78 W.

Figure 9 shows pulse repetition rate, pulse width, pulse energy, and peak power as a function of the absorbed pump power. Repetition rate increases linearly from 320 Hz to 12.7 kHz with absorbed pump power. The pulse width (FWHM) remains nearly constant of 2.5 ns with the absorbed pump power. Pulse energy increases from 20 to 31 μJ with the absorbed pump power and pulse energy increases slowly when the absorbed pump power is greater than 2 W, and pulse energy tends to remain constant when the absorbed pump power is higher than 2.5 W. The peak power of Yb:YSAG/Cr^{4+}:YAG passively Q-switched microchip laser increases from 9 kW to over 12 kW with absorbed pump power and tends to remain constant at high pump power level.

5. Conclusion

In conclusion, the optical properties of Yb:YSAG crystal were investigated and it has been found that the absorption and emission spectra are broader than those of Yb:YAG crystal owing to the substitution of Al^{3+} ions with larger Sc^{3+} ions. Continuous-wave and passively Q-switched Yb:YSAG microchip lasers have been demonstrated for the first time. 1.12 W continuous-wave laser output power was measured for T_{oc} = 5%, the corresponding optical-to-optical efficiency was measured to be over 30%. Laser pulses with 31 μJ pulse energy and 2.5 ns pulse width at repetition rate of 12.7 kHz were achieved. A peak power of more than 12 kW has been demonstrated with nearly diffraction-limited output beam (M^2 < 1.2). The laser performance can be further improved by adopting Yb:YSAG crystal doped with high Yb concentration and thin gain medium to make the good overlap between pump beam and laser beam for laser-diode end-pumped microchip lasers.

Acknowledgments

This work was supported by the 21st Century Center of Excellence (COE) program of the Ministry of Education, Science, Sports, and Culture of Japan. One of the authors (A. A. K.) wishes to acknowledge the Russian Foundation for Basic Research and the Russian Academy of Sciences. The authors thank Prof. Denis R. Hall from Heriot Watt University for his reading of the manuscript.

#92201 - $15.00 USD Received 28 Jan 2008; revised 18 Mar 2008; accepted 24 Mar 2008; published 1 Apr 2008